Resubmitted to Adv. Eng. Mats., Apr. 2025

Profilometry-based Indentation Plastometry Testing of Tungsten at High Temperature

JR Miller[†], PJ McKeown[†], H Qiu[#] & TW Clyne[#]*

[†] Plastometrex Ltd
204 Science Park, Milton Road
Cambridge CB4 0GZ, UK.

[#] Department of Materials Science
University of Cambridge
27 Charles Babbage Road
Cambridge CB3 0FS, UK.

Abstract

This work concerns application of PIP (Profilometry-based Indentation Plastometry) to pure tungsten, at temperatures up to 800˚C. PIP involves extraction of stress-strain curves from measured indent profiles, via (automated) inverse Finite Element Method (FEM) modelling. This metal is brittle at room temperature, but plastic deformation (with little work hardening) becomes prevalent above about 200˚C. PIP-derived curves are consistent with tensile results in this regime. For lower temperatures, PIP allows extraction of yield stress values and work hardening characteristics, but brittle fracture precludes this for tensile testing. Attention is paid to effects induced by exposure to air at high temperature, with both oxide layer formation and the absorption of oxygen being investigated. At 800˚C, a highly porous oxide rapidly forms, with approximately linear growth kinetics. However, this has little effect on measured indent profiles (and hence on inferred stress-strain curves), both because time at high temperature can be kept short during PIP testing and due to the weak and porous nature of the oxide. A check on the role of creep revealed that it was significant at 800˚C (for typical quasi-static strain rates), but had only a relatively minor effect on the PIP-inferred stress-strain curve.

Keywords: Indentation plastometry; oxidation; tungsten, high temperature.

1 Introduction

The PIP (Profilometry-based Indentation Plastometry) methodology is based on iterative FEM modelling of the indentation[1-6], converging on the stress-strain relationship (captured in a constitutive law) that gives optimal agreement between measured and modelled outcomes. There are important advantages[7-10] in using the indent profile, rather than the load-displacement curve, as the target outcome. A further advance has been the recognition that, if 'scale-independent' stress-strain relationships are being sought, then the volume being deformed must be large enough to be representative of the bulk - which usually translates into it containing a relatively large number of grains. There are also certain other requirements, such as a need[4, 11] to create plastic strains in the range of up to at least a few tens of % and a loading frame with a capacity in the kN range.

Several publications have covered the application of PIP to various materials, production procedures, applications and effects. These include welds[12], pipelines[13], additively-manufactured components[14, 15], metal matrix composites[16], effects of residual stress[17],

* tel: 0044 7919 856352: e-mail: twc10@cam.ac.uk

case-hardened layers[18], very hard metals[19] and porous metals[20]. There is also a review[21] that summarises various aspects of the methodology, including details of experimental procedures, theoretical background and how the FEM modelling is carried out. Furthermore, a recent publication[22] covers the development and usage of a high temperature stage, with a capability of up to 800˚C. The aim is to capture the plasticity of the sample, ideally with no creep effects. In practice, depending on material, temperature and test duration, the effects of creep on both PIP and tensile testing may be significant. This has been investigated, and reliably captured in models, for both 'creep-affected'[23] and 'creep-dominated'[24] conditions.

A material of particular interest for (quick and convenient) testing at high temperature is tungsten, partly because it is a candidate for plasma-facing walls of fusion reactors. Its high melting temperature, good thermal conductivity and microstructural stability under high irradiation fluxes make it particularly attractive for this highly demanding application[25-27]. It can undergo recrystallization, although this usually occurs only after extended periods at very high temperature[28, 29]. There are, however, several concerns about tungsten (and its alloys) in this context. One is that it tends to be brittle, particularly at ambient temperature. Reported tensile stress-strain curves[30-32] generally indicate that fracture occurs at very low strain at room temperature – there is usually little or no plasticity. Unsurprisingly for such brittle material, the failure stress is variable (and has little intrinsic significance), but is usually in the range 400-800 MPa. It has been reported[33] that extensive prior heat treatment can raise the ductility to at least a few %. In general, however, most published work indicates that tungsten is almost ideally brittle (in tension) at room temperature, with little or no information available about how plasticity might develop if fracture could be avoided.

However, the properties change at higher temperature. Most reports based on tensile testing[30, 32, 34] indicate that, while the yield stress remains at around 400-600 MPa as the temperature is raised, the strain at necking (peak in a nominal plot) tends to rise slightly, perhaps reaching about 5-10% at 500˚C. In fact, one report[31] indicates levels of several tens of % at above 1000˚C, although this is presented in terms of 'ductility' (nominal strain at fracture), which actually depends on sample dimensions. In general, previous reports indicate that, while plastic deformation does occur above about 200˚C, there is little or no work hardening over the complete temperature range.

A caveat should, however, be added in this context, regarding compression testing - an obvious way to seek information about the plasticity characteristics of brittle materials. Some such testing[35, 36], carried out at 800˚C, indicates that, from a yield stress of about 400 MPa, significant work hardening does apparently occur, giving a stress of around 700 MPa at a strain of about 30%. However, these are nominal stresses and strains. For a nominal strain of (-)30%, a nominal stress of (-)700 MPa converts to a true stress of only (-)490 MPa (at a true strain of (-)35%). If the same material were tested in tension, it also would yield at 400 MPa, but it would then be likely to neck well before a true strain of (+)35% had been reached. This can be seen from the fact that, for a true strain of (+)35%, which equates in tension to a nominal strain of (+)42%, the nominal stress at the point where the true stress had reached (+)490 MPa would in fact be (+)345 MPa. In practice, the peak in a tensile nominal stress-strain curve for this material (and hence the onset of necking) would probably come at about 420 MPa (UTS), at a strain of just a few %. In other words, completely different (superficial) impressions of the amount of work hardening can be obtained on comparing nominal plots in tension and compression. In view of the attractions of compression testing in avoiding fracture, this is a significant point for materials such as tungsten. It illustrates the dangers of presenting only nominal stress-strain curves (in tension or compression),

particularly for cases in which the strains become relatively high. There are also certain other difficulties with compression testing, if the aim is to obtain accurate information about yielding and work hardening, most of them associated with the effects of friction between sample and platen[19].

One feature of tungsten is that it has a relatively high solubility for oxygen[37-39] – an interstitial solute that can cause embrittlement. As an interstitial, its diffusion rates tend to be rapid. For example, theoretical estimates[40] of diffusion coefficient values are about 10^{-11} m^2 s^{-1} at room temperature and 10^{-8} m^2 s^{-1} at 800˚C. (Corresponding diffusion distances after one minute are about 25 μm and 0.8 mm.) Furthermore, there is a strong tendency for oxides to form at high temperature – usually this is predominantly the Trioxide (WO_3), although there are several variants of it, with different crystal structures and stoichiometries[41]. There are reports[42] that the kinetics of oxide growth are quite rapid, and often approximately linear, although growth rates can be reduced by alloying[43]. A review[44] is available that covers the issue of protecting tungsten from oxidation when it is being used for plasma-facing walls in fusion reactors. It is certainly clear that such components may become exposed to oxygen at high temperature and that this could lead to significant degradation of properties. Dispersed oxide within tungsten is sometimes regarded as providing a 'strengthening' mechanism[45], but in general there is a marked tendency for the material to become more brittle as oxygen contents are raised. Such characteristics can create problems both in terms of performance under service conditions and for mechanical testing procedures.

One of the advantages of PIP testing is that both yielding and work hardening characteristics can be obtained, even for brittle materials (that would be likely to fracture at a low strain during tensile testing). This is in principle true for all indentation-based procedures and a number of papers have covered such work on polycrystalline tungsten[46-53], carried out at ambient and/or elevated temperature. However, these studies were exclusively based on use of nano-indenters (with penetration depths of the order of 1 μm or less), which have associated difficulties of thermal drift and various 'size effects'. One investigation[8] did involve 'micro-indentation', using a spherical indenter with a radius of 0.25 mm and a penetration depth of around 25 μm, but this related only to single crystals of tungsten. None of these studies resulted in the extraction of stress-strain curves, or even yield stress values (apart from the potential for estimating it from a hardness number). Reported hardness values[46, 47, 49-53] cover a wide range, partly due to size effects, but in general they are of the order of 5-20 GPa at room temperature, falling to about 1-4 GPa at temperatures of 400-1000˚C. Obtaining a yield stress from a (Vickers) hardness number (expressed in MPa or GPa) is not a reliable procedure[54], but it is common to take it as having an approximate value of $H_V/3$. This leads to yield stress estimates that bear little relation to reality and it's difficult to avoid concluding that none of these studies have produced useful information about the stress-strain curves of polycrystalline tungsten.

Harris and co-workers[48, 50] reported that creep affected their observed indentation outcomes for tungsten at 800˚C, although it should be borne in mind that various types of (machine-affected) time dependence commonly arise during nano-indentation at high temperature. For tungsten at 800˚C (homologous temperature ~0.29), the general expectation might be that this is low enough to ensure that creep is negligible. However, such expectations commonly refer to steady state rates of creep, whereas it's primary creep that is likely to influence indentation outcomes (and also those from high temperature tensile testing, aimed at obtaining plasticity relationships). As a broad generalization, deformation rates[55-57] during primary creep are commonly at least two orders of magnitude higher than those in the steady

state regime, particularly at relatively high stress levels (close to the yield stress). The possibility of creep affecting indentation outcomes at elevated temperatures[22] should always be borne in mind. There has been work[58, 59] on the creep characteristics of tungsten, although much of this has been focussed on very high temperatures (>~1,300˚C) and on steady state rates of creep. Among the general conclusions are that recrystallization can have a strong effect and that exposure to oxygen can sharply reduce the creep resistance (in terms of promoting rupture).

The focus of the current paper is on using PIP to obtain stress-strain characteristics for tungsten over a range of temperature (up to 800˚C), with attention being paid to the possibility of oxygen-related effects and creep.

2 Materials and Test Procedures

2.1 Material

2.1.1 Composition and Supplier

The testing programme concerns a single material – nominally pure tungsten, supplied as 3 mm thick plate by Molybdenum Tantalum Tungsten Ltd. (Wickford, Essex). The chemical analysis provided by the supplier is presented in Table 1. These impurity levels are all relatively low. In particular, the oxygen content is about 60 ppm and the total interstitial content (O, C & N) is about 170 ppm. However, no information is available about the origin of these values and they may just be notional (upper limits).

Composition (wt %)							
Ni	Si	Fe	Mo	O	C	N	W
0.003	0.006	0.009	0.016	0.006	0.007	0.004	bal.

Table 1 Composition of the tungsten plate.

2.1.2 Microstructure

The microstructure was examined using optical microscopy. Samples were ground to 1200 grit and then polished down to 1 μm diamond paste, using conventional procedures. Microstructural features can be seen in the optical micrograph of Fig.1, which is a section parallel to the free surface of the plate. (Very similar structures were seen in other sections.) The material is free of obvious porosity, has no clear directionality and comprises a mixture of original (dark) and recrystallized (light) grains. There is just a single (bcc) phase present.

Details of the manufacturing procedure are not available, but it probably involved consolidation of tungsten powder (with the particle size ranging from a few microns up to several tens of microns), followed by a sintering operation (with no hot rolling). The sintering was probably carried out at around 1300˚C, leading to the observed partial recrystallization. This is broadly consistent with previously-reported microstructures[28, 60], as well as with the observations made here. For present purposes, it's not really necessary or appropriate to investigate microstructural characteristics of the as-received material in greater depth than this. The main features are fairly clear. However, there is interest in the effects of exposure to oxygen (at high temperature) and an investigation of these is described below.

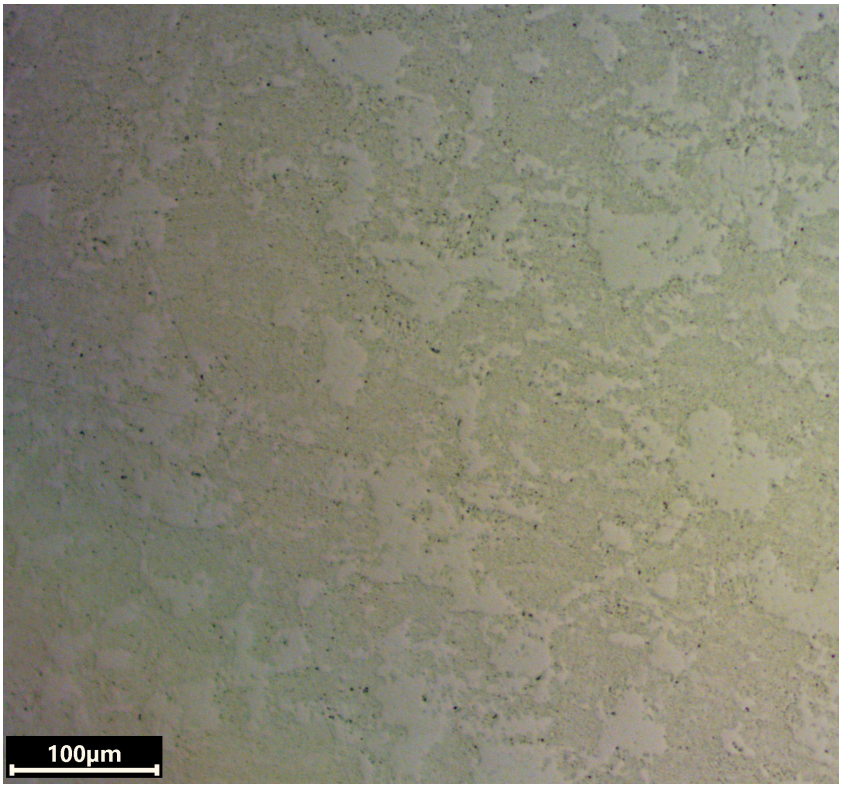

Fig.1 Optical micrograph of as-received tungsten.

2.2 Heat Treatments and Oxidation Countermeasures

2.2.1 Heat Treatments and Environments

Samples for heat treatment were in the form of small squares cut from the plate (7 mm x 7 mm x 3 mm). These were pushed into a tube furnace that had reached the temperature concerned. After exposure to static air for the period concerned, samples were then pushed out of the furnace in a similar way. Some of the samples were then used for measurement of their oxygen and nitrogen contents – see §2.2.3. Others were mounted and polished, for examination of transverse sections in the optical microscope. This work was aimed at investigating the formation of oxide films on the free surfaces.

2.2.2 Gold Coatings

A possible approach to inhibition of oxidation is to provide a thin, uniform coating of some sort over the complete surface of the sample, or at least over the top surface of a PIP sample, where the testing is localized. The objective is to create a layer that is fully dense, and hence impermeable, does not itself become oxidized and will deform plastically during indentation without affecting the indent size or shape in any way. Certain points may be noted concerning the suitability of gold for protection against high temperature oxidation of metals. It is not expected to itself oxidize at all, even in air at very high temperature – such a reaction is not thermodynamically favoured. Also, with a melting point of 1,064˚C, it should not melt in the temperature regime of interest here (although it clearly isn't suitable for protecting tungsten when employed as a plasma-facing wall, with surface temperatures potentially reaching 2,000˚C).

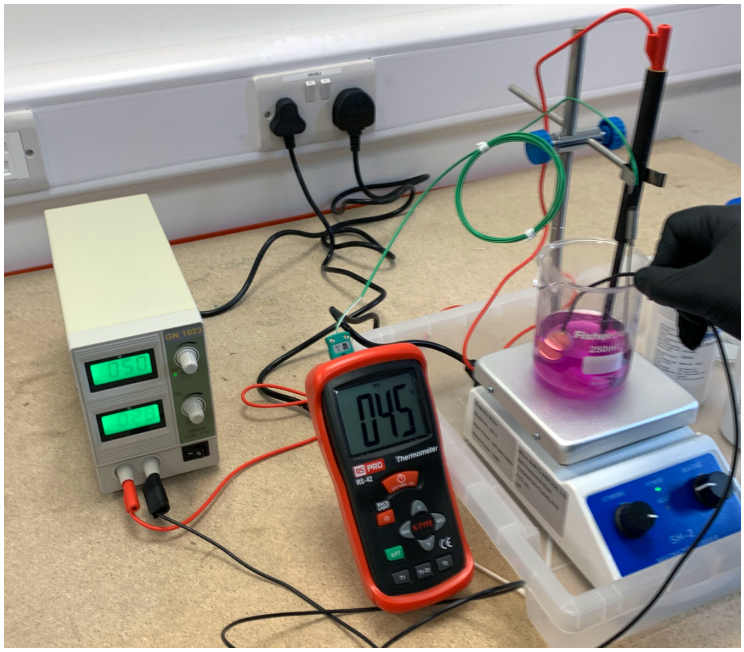

Fig.2 Photo of the set-up being used for electroplating a sample with a gold coating.

Layers of gold were created using an electroplating (EP) procedure[61, 62]. In general, such coatings adhere well to most metals, are fully dense and mechanically robust. For example, it has been shown[63] that electroplating steel components with gold layers several μm in thickness gave improved lubrication under conditions of heavy wear and were extremely durable. No publications have been found that refer to electroplated layers of gold on tungsten, although there has been work[64, 65] involving thin (PVD) coatings. These are unlikely to be suitable for present purposes, since they tend to agglomerate quickly at high temperatures.

In the present work, the electroplating was done using a Golden Solution GN1023 Gold Plating Kit. The electrolyte was a Gold Tank Plating solution supplied by Spa Plating. A photo of the electroplating set-up is shown in Fig.2. Small squares (7 mm x 7 mm x 3 mm) were electrically connected as cathodes via a copper wire wrapped once around the sample. The total surface area was about 180 mm^2. Samples were fully immersed in an electrolyte (initially) containing 8 g $litre^{-1}$ of gold ions. The electrolyte was warmed to just above 40˚C and stirred manually throughout. The anode was a graphite rod. The applied voltage was 5 V, which typically created a current in the circuit of about 0.4 A. Monitoring of coating thickness was carried out by weighing the sample before and after the electroplating operation, although some transverse sections were also examined in an optical microscope as a check on this. These samples weighed just under 3 g and the increase in weight due to the gold coating was about 3.5 mg per micron of coating thickness. The measured deposition rate was found to be about 0.7 μm $min.^{-1}$, although this rate can fall as the electrolyte becomes depleted of gold ions. The results presented here relate to coatings about 4 μm in thickness.

Reaction between gold coating and sample might be conceivable in some cases, but in general gold is inert in contact with other metals, provided both remain solid. However, it's certainly possible for species from the sample to dissolve in gold, and potentially to diffuse through a gold layer. For example, the diffusivity[66] of Fe in gold at 700˚C is about 5 10^{-15} m^2 s^{-1}, giving a diffusion distance of several microns after a period of 20 minutes. Elements such as Fe have a high solubility in gold. The gold-tungsten phase diagram[67], however, indicates that gold has little or no solubility for tungsten. The diffusivity of tungsten

in gold (at temperatures of up to 800˚C) is unknown, but is likely to be relatively low. Significant migration of tungsten through a gold layer (assuming that it is coherent and pore-free) therefore seems unlikely. The solubility of oxygen in gold is very low – estimated[68] to be about 1 ppm at 700˚C. It's an interstitial solute, so its diffusivity is high, but this low solubility means that there should be little or no transport of oxygen through a gold layer. From a mechanical point of view, pure gold is very soft and ductile, particularly at elevated temperatures, so the layer is likely to simply conform to the indent shape dictated by the sample, at least for thickness levels of no more than a few microns.

2.2.3 Measurement of Internal Oxygen Content

Measurement of the oxygen contents was carried out by Special Testing Ltd (Sheffield), on small sections of plate (10 mm x 10 mm x 3 mm). This was done using a LECO 736 series machine. A pre-weighed sample is heated in an enclosed graphite crucible, releasing O_2, which is reduced to CO and CO_2, and N_2. These gases are extracted and the CO is converted to CO_2, which is then analysed using an infra-red cell. Publications, such as the paper of Kipphardt et al.[69], provide details of the techniques involved.

2.3 Mechanical Testing

2.3.1 PIP Testing

Detailed outcomes of PIP testing at high temperature (HT-PIP), applied to several alloys at up to 800˚C, have been published[22], with a wide range of comparisons made between PIP-derived stress-strain curves and those from tensile testing. That paper also provides full technical details of HT-PIP testing procedures. In the present work, samples were in the form of square pieces of plate (10 mm x 10 mm x 3 mm). The standard indenter penetration velocity was 3 μm s^{-1}, although, for the higher temperatures, tests were also carried out with a lower velocity (to check on whether creep was affecting the outcome). The heating period naturally depends on test temperature, but was about 10 minutes for the highest (800˚C) - see §4.1.2. One point to note concerning PIP testing is that the elastic constants of the material are input data for the model. In the present case, these were specified in the form of the Young's modulus being 400 GPa and the Poisson ratio being 0.3. (The effect of the exact values used on the inferred plasticity characteristics is relatively small.)

2.3.2 Tensile Testing

The tensile testing was carried out using an Instron 3369 loading frame, with a Severn Thermal Solutions Furnace. The samples were produced by Electro-Discharge Machining (EDM) of the W plates, carried out by EDM Precision Technologies Ltd. The reduced section length was 30 mm, with a width of 3.1 mm, and the clip gauge length was 25 mm. The ceramic knife-edges of the clip gauge come through a small slot in the furnace wall, while three thermocouples (to be touching the sample within the gauge length) are introduced from the other side of the furnace. Samples were heated at 20 K min^{-1}. There was a 20 minute stabilization period prior to the start of the test. The standard displacement rate during loading was 10 mm min^{-1}, corresponding to a strain rate of about 7 10^{-3} s^{-1}. For the highest temperature, tests were also carried out with a slower strain rate, to check on whether creep was affecting the outcome.

3 Oxidation Characteristics

Information about the oxidation characteristics at 800˚C, without and with gold coatings, is provided by the optical micrographs in Fig.3, while the plot of Fig.4 gives an indication of the

growth kinetics at 700˚C and 800˚C. There is a suggestion of an oxide on the as-received material (even after polishing), although it's apparently no more than a micron or so in thickness. It certainly thickens rapidly at 800˚C, reaching several tens of microns after an hour. Even after 15 minutes, it is about 10-20 μm thick. Furthermore, it can be seen in Fig.3 (particularly Fig.3(e) and Fig.3(f)) that this oxide contains high levels of porosity – which is almost certainly inter-connected. The layer of porosity at the interface between oxide and metal is probably due to detachment during the grinding and polishing, but it seems clear that there is also a lot of porosity in the interior of the oxide layer.

Consistent with this is the observation that the rate of growth remains high. In fact, the plot in Fig.4 suggests that the growth kinetics are at least approximately linear. This is expected if air can penetrate readily through the network of porosity. There is also broad consistency with previous publications[42, 43]. It is clear in Fig.4 that the effect of temperature is quite strong, with the (linear) growth rate being lower by a factor of about 3 at 700˚C. (Measurements made at 600˚C indicated that very little oxide was formed at this temperature, even after 2 hours.)

The possible presence of such an oxide layer should be noted in view of its potential effect on HT-PIP testing, since it could affect the residual profile – particularly in the pile-up region immediately adjacent to the indent. On the other hand, one advantage of HT-PIP testing is that the heating and thermal equilibration period can be very short. For example, HT-PIP testing at 800˚C can be carried out such that the period prior to the test spent above, say, 700˚C, can be limited to just a few minutes[22] – see §4.1.2. Oxide formation may thus be quite limited, even for a case (such as tungsten at 800˚C) that exhibits rapid growth.

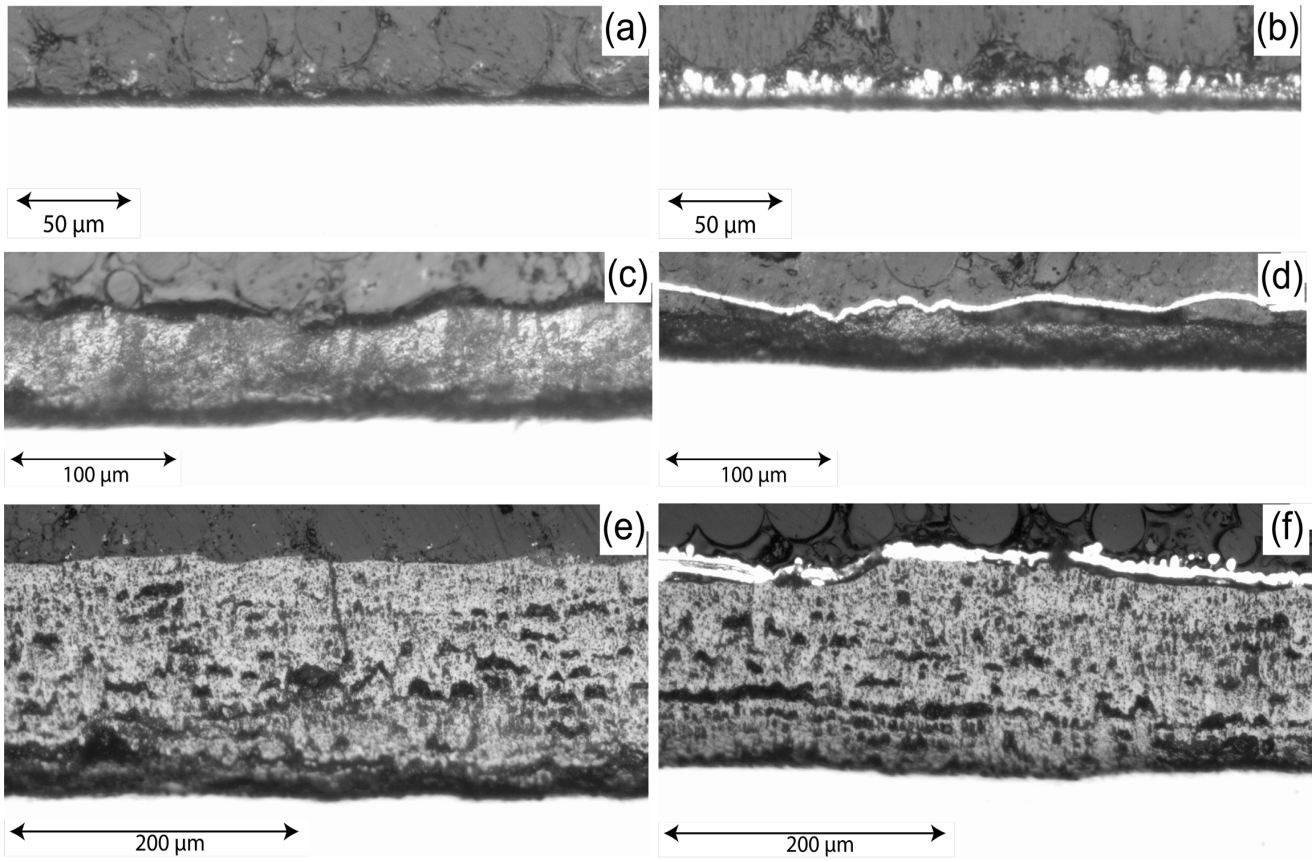

Fig.3 Optical micrographs of transverse sections, showing samples in (a) as-received, and (b) as-coated states, while (c) and (d) show such samples after 30 minutes at 800˚C and (e) and (f) after 2 hours at 800˚C.

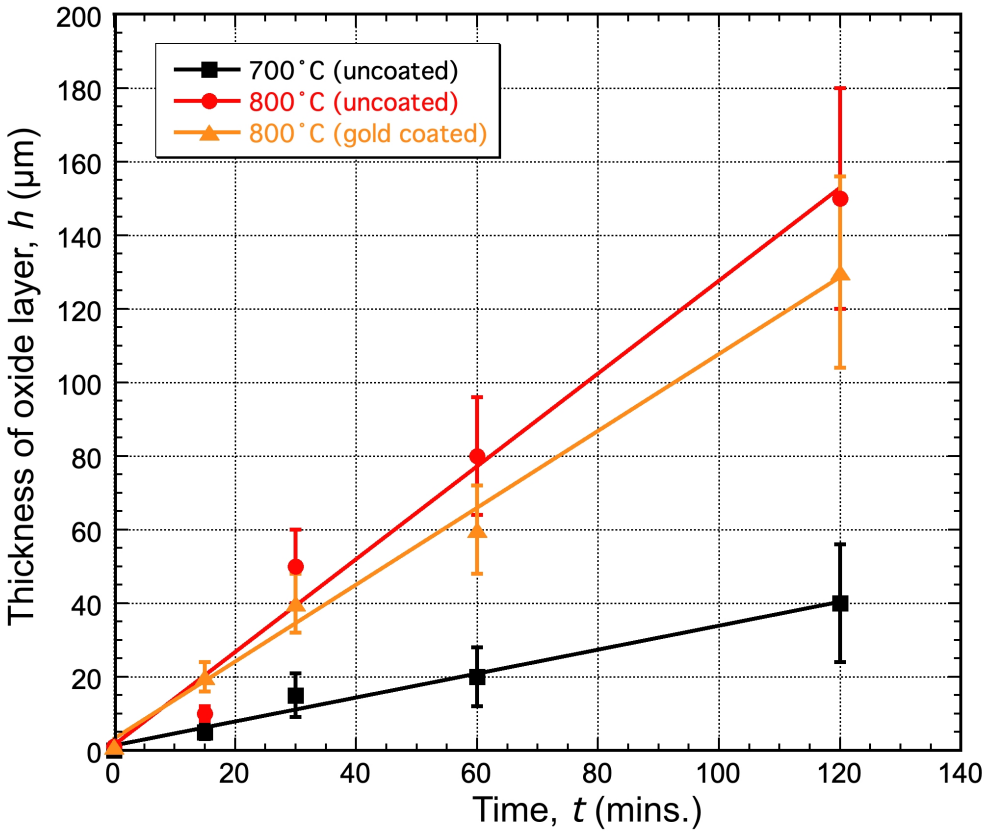

Fig.4 Plot of oxide layer thickness (measured on optical micrographs) as a function of time, for tungsten heat treated in air at 700˚C and 800˚C, with the latter having been carried out without or with gold coatings (about 4 μm in thickness).

A further point that emerged from these tests is that the gold coatings had little or no effect on the rate of oxide growth. This can be seen in Fig.4 for the 800˚C data, which indicate that, within experimental error, the growth rate is about 1 μm $min.^{-1}$, with or without the coating. It's also clear from the micrographs in Fig.3 that the oxide forms on the inside of the coating. This appears to suggest that oxygen can pass through the gold. In practice, it seems likely that the gold layer is not continuous or coherent, rather than it all being permeable to oxygen. The electroplating procedure doesn't appear to be very reliable for tungsten and the integrity of the coating was rather variable. Prediction of the efficiency of producing (electroplated) gold coatings on different metals is not easy, since it presumably depends in a complex manner on the electrochemistry of the surface region. There is certainly some variability in the appearance of these coatings, but they don't seem to be reliably continuous or coherent. If air can pass through such a coating, even if only in relatively few locations, then the highly porous nature of the oxide will allow it to redistribute laterally, leading to growth rates that are similar to those for an uncoated surface.

No chemical analysis of the oxide layers has been carried out, but it seems likely that it was all WO_3 – with or without some depletion of oxygen content. It is certainly well-established that this oxide is commonly formed. Also, it is worth noting that the Pilling-Bedworth ratio for WO_3 is about 3.4 – so oxidation of the tungsten is accompanied by a large increase in volume. This may be relevant to the high observed levels of porosity. Also potentially relevant is the fact that WO_3 undergoes phase transformations during heating and cooling[41], with the monoclinic form being stable up to 330˚, the orthorhombic structure from there to 740˚C and the tetragonal above that temperature. A tendency for WO_3 to be highly porous, and potential advantages of this in certain functional devices, have been studied[70, 71]. It may also be noted

that, depending partly on viewing conditions, there were cases in which the oxide appeared to comprise two distinct layers, with contrast between them (sometimes appearing to have different colours). It seems likely that both are nominally WO_3, but one of them is somewhat depleted in oxygen. There are reports of such effects in the literature[72, 73].

Sample	O content (ppm)
W plate (as-received)	16
W plate (30 mins. @ 800˚C)	20
W plate (2 h. @ 800˚C)	32
Au-coated W plate (30 mins. @ 800˚C)	31
Au-coated W plate (2 h. @ 800˚C)	29

Table 2 Measured oxygen contents in tungsten samples after different heat treatments.

Further information about the effects of exposure to air is presented in Table 2, which shows measured internal O contents (after any oxide layer had been removed by a grinding operation), for heat treatment at 800˚C, with and without gold coatings. These values show little correlation with the 60 ppm value quoted by the supplier for as-received material (being all considerably lower). However, while there are indications in these results that the O content can be raised by a heat treatment, the main conclusion here is that these levels are all low. (It is unclear how the value quoted by the supplier was obtained and it may just be a generally expected upper limit.) It would also appear that the gold coatings do little or nothing in terms of inhibiting penetration of oxygen. As for the results relating to oxide layer thickness, this may be attributable to the gold coatings having poor integrity. It is in any event clear that the main effects of exposure to air at high temperature relate to the formation of oxide layers, rather than to penetration of O into the interior of the sample.

4 Mechanical Properties

4.1 PIP Indent Profiles

4.1.1 Measured and Modelled Profiles

Details of the FEM model, including the procedure for convergence on the stress-strain relationship giving optimal agreement between measured and modelled outcomes (indent profiles), are provided in previous publications - particularly the review article[21]. The justification for selecting the Voce relationship as the constitutive law describing the (true) stress-strain relationship is also described there in some detail. The only arbitrarily-adjustable parameter in the procedure is the value of the friction coefficient between sample and indenter, although the outcome is not very sensitive to its value (in the expected range of about 0.1-0.3). For the present work, the value used was 0.225. This issue is also explored in the review article.

A typical comparison between measured and (best fit) modelled indent profiles is shown in Fig.5. The agreement is close (and the sensitivity of the modelled profile to the stress-strain curve is relatively high). A feature of this profile, and of all those in the current study, is a large pile-up height – almost a third of the central depth in this case. In general, this is reflective of a low work hardening rate. (Work hardening tends to act against the localised creation of large plastic strains, which are associated with high pile-ups.) In fact, the work hardening rate of this tungsten plate is low across the range of temperature – see §4.2.1. A further point to note

here is that this experimental profile was produced after heating to 800˚C – a case for which an oxide layer of significant thickness (~20 μm) was present during indentation. Nevertheless, the profile is clearly smooth (in the pile-up region) and there is no evidence suggesting that pile-up formation has been suppressed in any way. This is discussed in §4.1.2 below.

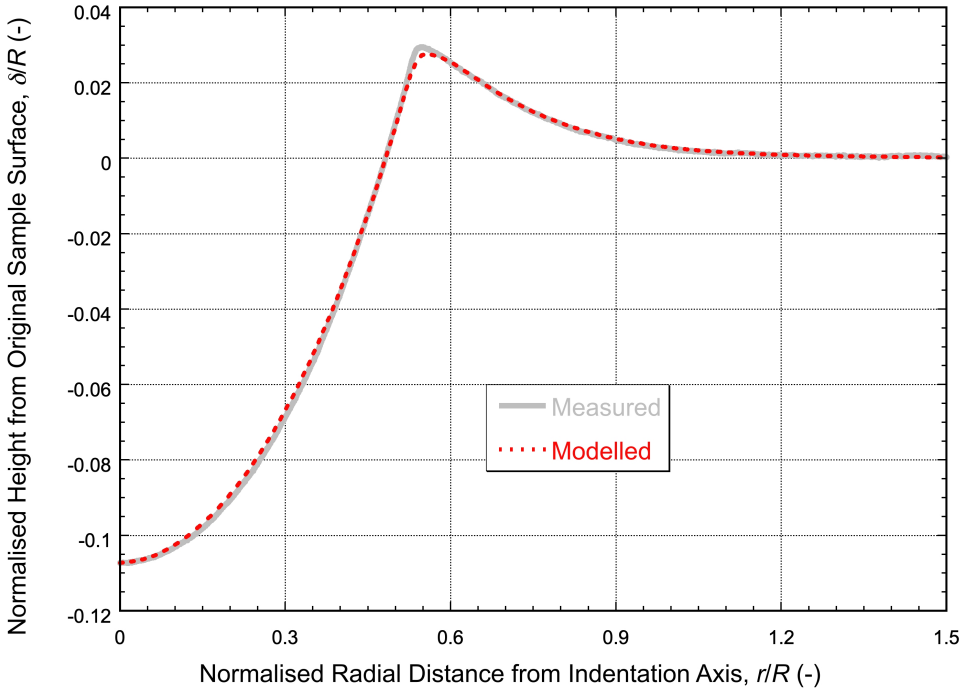

Fig.5 Measured and modelled profiles for an uncoated tungsten sample indented at 800˚C (with a load of 1.392 kN).

4.1.2 Effects of Oxide Films

There is potential concern that an oxide film on the sample could affect the measured indent profile and hence the inferred stress-strain curve. This could lead to a reduction in pile-up height, or even the creation of irregularities in this region (due to fragmentation of a relatively thick oxide layer). In fact, it can be seen in Fig.5 that the measured profile is perfectly smooth, and also that the pile-up height is relatively large, even for this case of 800˚C, for which a relatively thick oxide layer was present. Nevertheless, there is interest in examining the near-surface region after indentation, and correlating this with the thermal history of the sample.

Some information is presented here concerning indentation at 800˚C. Firstly, Fig.6 shows the thermal history of the sample, before and after indentation. If the time spent between, say, 700˚C and 800˚C is taken as a pointer towards oxide film thickness, this is about 6-7 minutes prior to indentation, but only about 2 minutes during the subsequent cooling. From the information in Fig.4, a broad expectation would be that the oxide film thickness had reached about 15-20 μm by the time that indentation took place, with little thickening afterwards.

This expectation is consistent with the micrograph shown in Fig.7. Measurements made of the oxide thickness in the pile-up region (and outside of it) indicate about 22 μm, whereas in the region that was in contact with the indenter ball it is about 18 μm (with some indications that it may have been compressed so as to eliminate most of the porosity). It might have been expected that an oxide film with a thickness of the order of 20 μm could inhibit pile-up formation, at least slightly. However, this doesn't appear to have happened in the present case - pile-up heights are quite substantial (at about a third of the central depth). This is reflected in low rates of work hardening in the inferred stress-strain curves - see below. A likely explanation is that the high porosity level in the oxide rendered it mechanically weak,

such that it had little or no effect on the creation of the pile-up. It is worth noting in this context that tungsten is fairly strong, even at high temperature, making it less susceptible during pile-up formation to effects induced by an oxide.

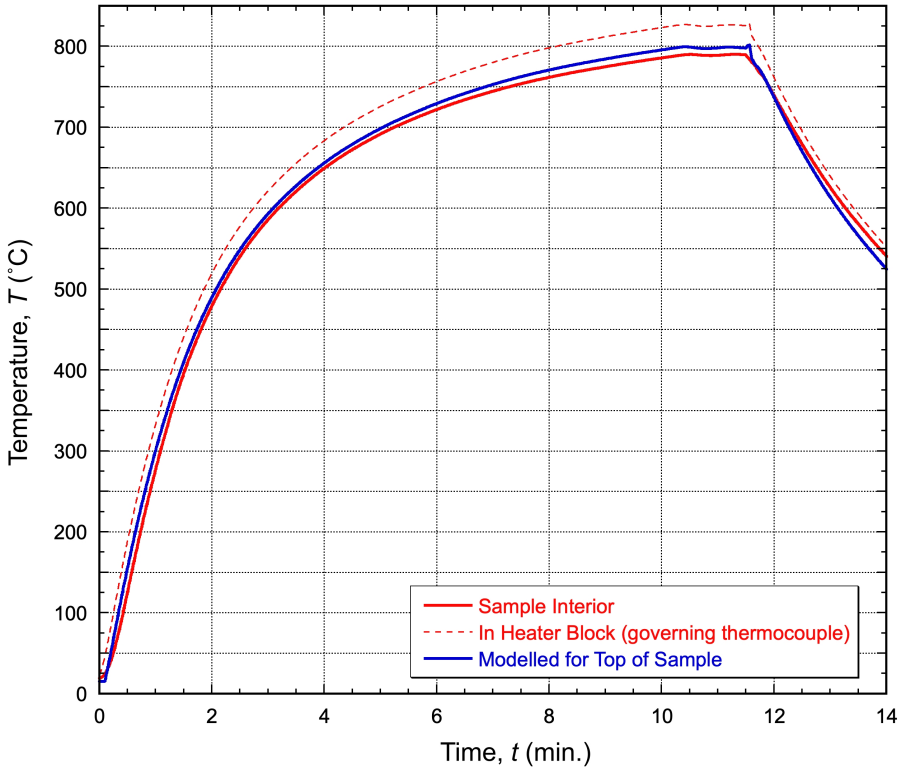

Fig.6 Thermal history of the sample surface before and after indentation of an uncoated tungsten sample at 800˚C.

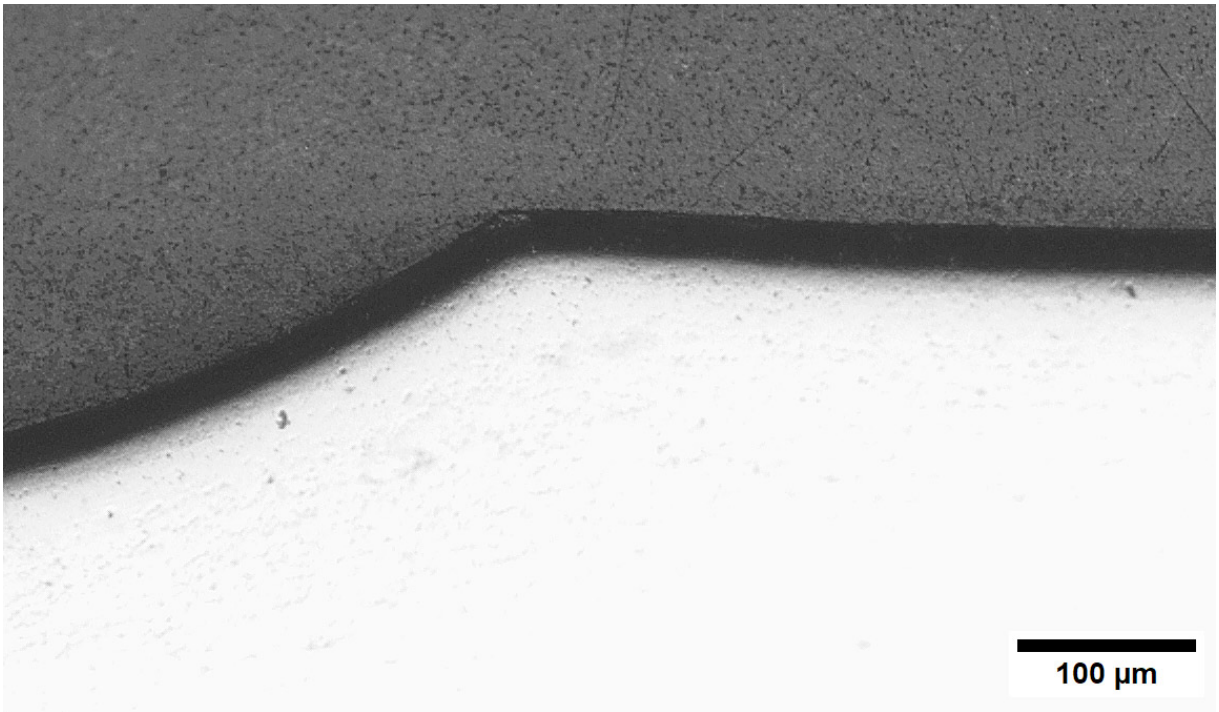

Fig.7 Optical micrograph of a transverse section in the vicinity of the pile-up region of an indent created during a HT-PIP test at 800˚C.

4.2 Stress-Strain Curves

4.2.1 PIP-Derived and Tensile Outcomes

The immediate outcome of the PIP tests - that is, the optimized sets of Voce parameters, plotted as true stress – true strain curves (with the elastic strain also added), is shown in Fig.8. The yield stress values can be seen, as can the nature of the work hardening behaviour. (The latter can be seen more clearly in plots of this type, compared with nominal stress-strain curves.) The yield stress progressively drops from about 1,300 MPa at room temperature to around 500 MPa at 800˚C (although in fact it has dropped to ~600 MPa by 300˚C). It's also noticeable that the rates of work hardening are low, with the true stress rising by about 300 MPa over a strain range of about 15% at room temperature, but there being very little rise in the 'flow stress' at temperatures of 200˚C and above.

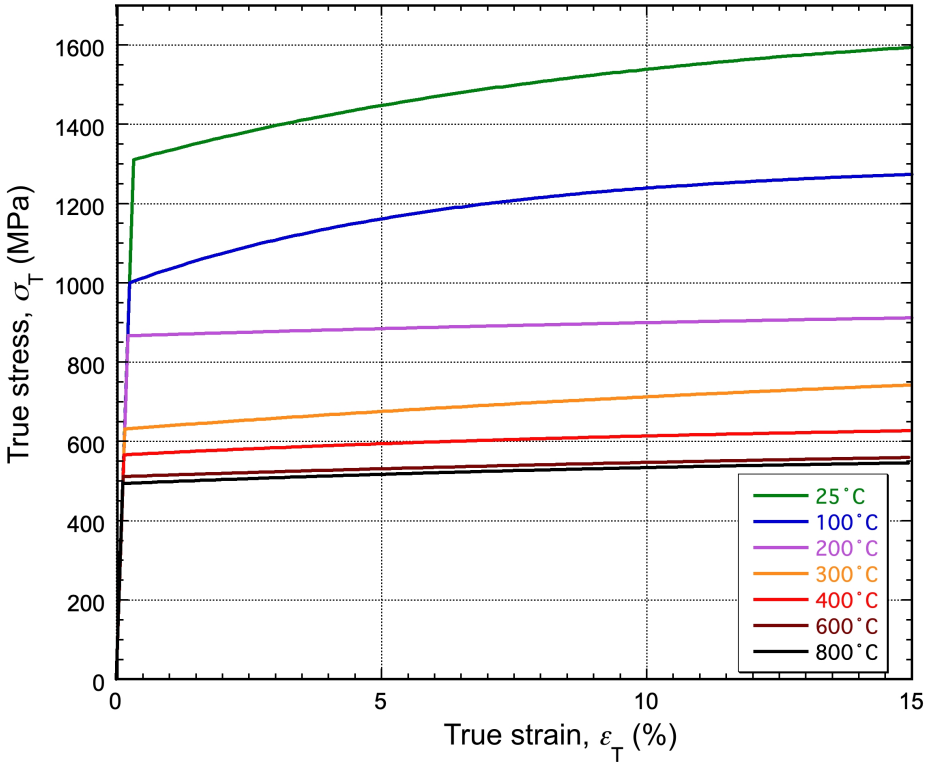

Fig.8 PIP-derived true stress - true strain curves, obtained using an indenter penetration velocity of 3 μm s^{-1}.

Comparisons between PIP and tensile outcomes are conventionally presented as nominal stress – nominal strain plots (although, as noted above, the actual plasticity characteristics of a material can be seen more clearly in a true plot). The set of tensile stress-strain curves obtained in the current work is shown in Fig.9, together with corresponding PIP curves. Some caveats are needed here. A first point to note is that the PIP-derived plots, which have been obtained by converting the true plots using the standard analytical expressions, are shown only up to the peak in the curve (where, according to the Considère criterion, the onset of necking is expected). In some of these cases (at the higher temperatures), this is predicted to occur at very low strains - indicative of little or no work hardening (as can be seen in Fig.8). The tensile curves are shown beyond this point, but they are not really meaningful in this regime (since the measured strain is entirely dependent on how the neck develops). Secondly, the tensile behaviour at room temperature, and at up to 200˚C is almost ideally brittle. The only information from tensile testing in this regime is a fracture stress. Moreover, this value is virtually meaningless in terms of plasticity characteristics, and is likely to vary if tests are

repeated. (Just single values are shown in the plot.) In this temperature range, no comparison is possible in terms of yield stress or rates of work hardening.

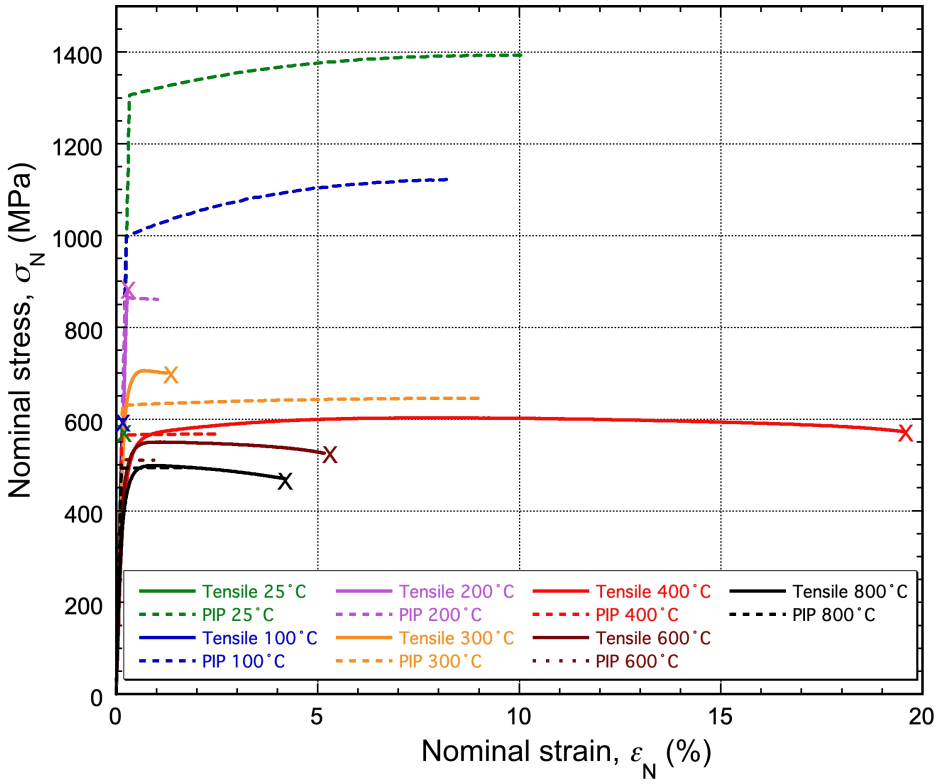

Fig.9 Comparison between nominal stress-strain curves from tensile and PIP testing, with the latter shown only up to the onset of necking (peak in the curve). These tensile tests were carried out with a strain rate of 7 10^{-3} s^{-1}.

For temperatures above 200˚C, however, there is good consistency, with the tensile yield stress progressively falling with increasing temperature, but over a fairly narrow range (~700 to 500 MPa, as the temperature is raised from 300˚C to 800˚C). Moreover, these tensile curves also indicate little or no work hardening. Strains at the onset of necking (peak in the plot) are low, while the ductility values (nominal strain at fracture), as indicated above, are not really meaningful – they are dependent on sample dimensions, since this affects the relative significance of the straining that takes place within the neck.

A summary comparison is shown in Fig.10, in which yield stress (YS) and ultimate tensile stress (UTS) values obtained by both PIP and tensile testing are plotted as a function of temperature. This plot covers only tensile results from the current work, although it may be noted that they are closely consistent with those from the two papers in the literature[31, 32]. There is clearly little or no work hardening at temperatures above about 200˚C (with brittle fracture preventing access to the yielding and work hardening characteristics at lower temperatures). For the brittle facture cases, and taking account of the values reported in those two papers, the wider error bars reflect the expected variability. All of the reported values fall in the approximate range 400-800 MPa, probably dependent mainly on the presence of surface flaws and possibly on gripping and alignment issues. It's clear that the exact value obtained in any particular test is of little or no significance.

It can be concluded that PIP is giving good consistency with tensile outcomes in the temperature range in which significant plasticity occurs, and it also seems justifiable to have confidence in the PIP outcomes for temperatures at which the tensile behaviour is entirely brittle. This capability of PIP testing is worthy of note (particularly since there are certain

difficulties associated with compression testing of very hard metals, as described in a previous paper[19]).

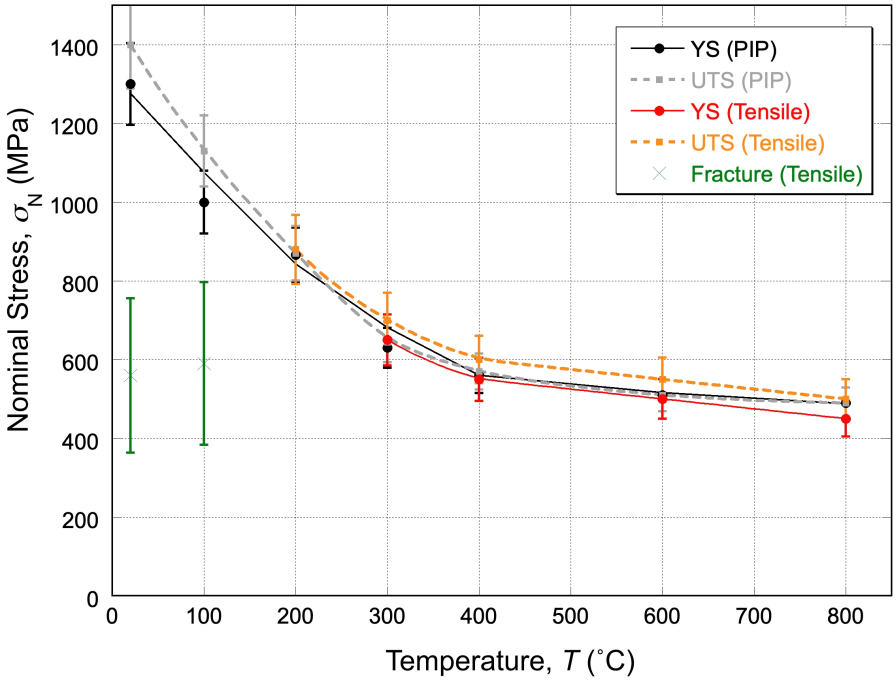

Fig.10 Comparison between YS and UTS values obtained by PIP and by tensile testing, as a function of test temperature.

4.2.2 Creep Effects

There is potential concern about creep (time-dependent) deformation affecting virtually any test aimed at obtaining stress-strain ('pure plasticity') curves, particularly at high temperature. This applies equally to PIP and tensile testing. Recent publications[23, 24] cover the details, and show that observed effects can be quantitatively explained. A rule of thumb is often expressed as creep probably being insignificant for homologous temperatures below about 0.4 (~1,200˚C for tungsten). However, as noted in the Introduction, this implicitly relates to strain rates in the steady state regime during creep (constant load) testing. The system does not approach any kind of steady state during either PIP or tensile testing – in fact, this applies to most loading configurations (except uniaxial tests at constant load and certain important commercial applications, such as turbine blades). If creep deformation is taking place during PIP or tensile testing, then primary creep, which is almost inevitably much faster than secondary (steady state) creep, may be making a contribution, particularly at the relatively high stress levels (~YS) that are generated during these tests. Of course, the net effect of such creep on the extracted stress-strain curve will depend on the duration of the test, but interest centres here on tests within the 'quasi-static' regime, which is often taken to cover strain rates in the approximate range of 10^{-5} – 10^{-2} s^{-1}. Extracted stress-strain curves will be independent of strain rate in this range only if creep effects are negligible. The bottom line, however, is that creep can in practice have an effect in cases for which the homologous temperature is well below 0.4. For example, it's been shown[23] that detectable levels of creep occur during both PIP and tensile testing of titanium alloys at room temperature, which corresponds to an homologous temperature of 0.15. Of course, creep resistance is often quite sensitive to microstructure, which doesn't figure in criteria based on the homologous temperature.

In the present work, a check has been made on the effect of creep by carrying out tensile tests at 800˚C with two different strain rates and PIP tests at the same temperature with two

different penetration velocities. Unlike a tensile test, stress and strain vary with location during PIP testing. The relationship between penetration velocity and the (spatial and temporal) distribution of the local strain rate is a complex one. However, for a particular case, it's possible via FEM simulation of the indentation to obtain an average value for the strain rate, weighted by the amount of deformation that takes place within different ranges of strain rate. This procedure is described in a previous paper[22]. There is no universal relationship between this average strain rate and the indentation velocity (although it is expected to be at least approximately linear in any particular case), since it does depend on the plasticity and creep characteristics. However, this dependence is not very strong and, at least to an order of magnitude, a proportionality constant can be identified that should be broadly valid across typical ranges of deformation characteristics. For the current work, which concerns an indenter with a radius of 1 mm and a penetration ratio of 10-20%, its value is approximately $5\ 10^{-4}\ \mu m^{-1}$. The average strain rates in these two PIP tests (with velocities of 0.3 and 3 $\mu m\ s^{-1}$) were therefore around $1.5\ 10^{-4}$ and $1.5\ 10^{-3}\ s^{-1}$. While these figures are very approximate, they're evidently of a similar order of magnitude to those involved in the tensile tests.

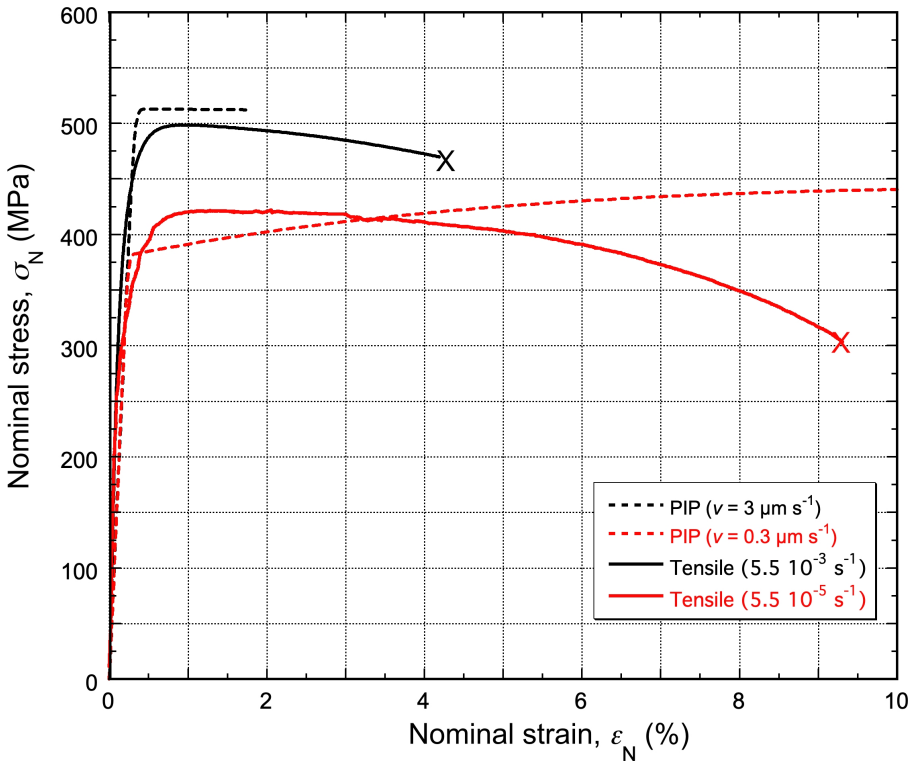

Fig.11 Nominal stress - nominal strain curves from tensile and PIP testing at 800˚C, obtained in both cases using two different strain rates.

The outcomes are presented in Fig.11, which shows nominal stress-strain curves for both tensile and PIP testing at 800˚C, with two different strain rates. For both types of test, the curves lie at lower stress levels for the slower strain rates (noting that it has been reduced by a factor of 100 for the tensile test, but only 10 for the PIP test). These curves therefore confirm that, for this temperature, creep could have a significant effect. However, the effect is not dramatic, with the stress reductions being moderate and the curve shapes remaining broadly similar. This is in contrast to what was observed in earlier work[22] for a number of ('creep-dominated') material / temperature combinations, where curve shapes became substantially different for the two types of test and neither was close to a genuine 'pure plasticity' relationship. Such cases have been successfully modelled[24] for tensile testing.

In the current work, even at 800˚C, the stress-strain outcome (from tensile or PIP testing) is likely to be reliable ('creep-free'), provided the testing is carried out at the 'standard' rates, so that both tensile and PIP outcomes can be taken to be close to such a relationship over the complete temperature range that has been covered. However, the fact that creep is starting to become significant at 800˚C should be noted: at higher temperatures, it is probable that stress-strain curves (from tensile or PIP testing) will become heavily 'creep-affected', such that results from the two tests will start to diverge (with neither being 'correct') even if the tests are done at 'standard' rates. Full understanding of the behaviour in this temperature range will require capture of the creep characteristics (including primary creep).

5 Conclusions

This work concerns application of the PIP methodology to plates of pure tungsten, at temperatures up to 800˚C. The following conclusions may be noted.

(a) Yield stress and work hardening characteristics have been obtained. The yield stress at ambient temperature is about 1,300 MPa, with some (fairly limited) work hardening. By 200˚C, the yield stress has fallen to about 900 MPa and by 600˚C to around 500 MPa. It remains at around this level up to 800˚C. The work hardening rate is very low for all temperatures above about 200˚C.

(b) These PIP-derived results are consistent with those from tensile testing, although comparisons are not possible below about 300˚C - when brittle fracture during tensile testing precludes the obtaining of plasticity-related characteristics. Since PIP testing is a much easier and quicker procedure, as well as having the capability to obtain plasticity characteristics in regimes inaccessible to tensile testing, it has considerable potential for study of materials such as tungsten.

(c) During exposure of samples to air at high temperatures, formation of oxide (WO_3) is rapid, with linear growth kinetics (and evidence of high porosity levels). At 800˚C, the growth rate is approximately 1 μm $min.^{-1}$. On the other hand, the rate of absorption of oxygen into the interior of the metal appears to be low.

(d) Rapid formation of an oxide layer on the surface of a sample prior to PIP testing is a potential cause for concern, since it could affect the indent profile and hence the inferred stress-strain curve. Furthermore, attempts to limit oxide growth by electroplating a thin layer of gold onto the surface were largely unsuccessful. However, the time spent at high temperature can be kept short during PIP testing, so that the oxide layer thickness is minimised. This appeared to ensure that inferred stress-strain curves were reliable, probably assisted by the weak and porous nature of the oxide.

(e) There is potential concern during high temperature PIP (and tensile) testing that creep could affect the stress-strain curve (such that the timescale of the test influences the outcome and it is not a reflection of 'pure plasticity' characteristics). It was found that, for testing at 800˚C, changing the indentation penetration velocity did affect the profile, and hence the stress-strain curve. A similar effect was observed when changing the strain rate of the tensile test. However, these effects were relatively minor and, at least over the temperature range covered in this work, the stress-strain curves obtained are thought to be more or less 'creep-free' (provided the tests at 800˚C are carried out at 'standard' rates). However, any test (tensile or PIP) carried out above 800˚C is likely to be quite strongly affected by creep.

Acknowledgements

Financial support for TWC has been provided by EPSRC, via Grant No. EP/I038691/1. Relevant support has also been received from the Leverhulme Trust, in the form of an Emeritus Fellowship (EM/2019-038/4).

References

1. J Dean, JM Wheeler & TW Clyne, *Use of Quasi-Static Nanoindentation Data to Obtain Stress-Strain Characteristics for Metallic Materials,* Acta Materialia, 58, **2010**, 3613-3623, https://doi.org/10.1016/j.actamat.2010.02.031.
2. DK Patel & SR Kalidindi, *Correlation of spherical nanoindentation stress-strain curves to simple compression stress-strain curves for elastic-plastic isotropic materials using finite element models,* Acta Materialia, 112, **2016**, 295-302, https://doi.org/10.1016/j.actamat.2016.04.034.
3. J Dean & TW Clyne, *Extraction of Plasticity Parameters from a Single Test using a Spherical Indenter and FEM Modelling,* Mechanics of Materials, 105, **2017**, 112-122, https://doi.org/10.1016/j.mechmat.2016.11.014.
4. JE Campbell, RP Thompson, J Dean & TW Clyne, *Experimental and Computational Issues for Automated Extraction of Plasticity Parameters from Spherical Indentation,* Mechanics of Materials, 124, **2018**, 118-131, https://doi.org/10.1016/j.mechmat.2018.06.004.
5. L Meng, P Breitkopf, B Raghavan, G Mauvoisin, O Bartier & X Hernot, *On the study of mystical materials identified by indentation on power law and Voce hardening solids,* Int. J. Mat. Forming, 12, **2019**, 587-602, https://doi.org/10.1007/s12289-018-1436-1.
6. H Xue, JX He, WN Jia, JL Zhang, S Wang, S Zhang, HL Yang & Z Wang, *An approach for obtaining mechanical property of austenitic stainless steel by using continuous indentation test analysis,* Structures, 28, **2020**, 2752-2759, https://doi.org/10.1016/j.istruc.2020.11.001.
7. J Lee, C Lee & B Kim, *Reverse analysis of nano-indentation using different representative strains and residual indentation profiles,* Materials & Design, 30, **2009**, 3395-3404, https://doi.org/10.1016/j.matdes.2009.03.030.
8. WZ Yao, CE Krill, B Albinski, HC Schneider & JH You, *Plastic material parameters and plastic anisotropy of tungsten single crystal: a spherical micro-indentation study,* J. Mater. Sci., 49, **2014**, 3705-3715, https://doi.org/10.1007/s10853-014-8080-z.
9. MZ Wang, JJ Wu, Y Hui, ZK Zhang, XP Zhan & RC Guo, *Identification of elastic-plastic properties of metal materials by using the residual imprint of spherical indentation,* Mat. Sci. & Eng. A, 679, **2017**, 143-154, https://doi.org/10.1016/j.msea.2016.10.025.
10. JE Campbell, RP Thompson, J Dean & TW Clyne, *Comparison between stress-strain plots obtained from indentation plastometry, based on residual indent profiles, and from uniaxial testing,* Acta Materialia, 168, **2019**, 87-99, https://doi.org/10.1016/j.actamat.2019.02.006.
11. TW Clyne & JE Campbell, *Testing of the Plastic Deformation of Metals*. 2021, Cambridge, U.K.: Cambridge University Press.
12. W Gu, JE Campbell, YT Tang, H Safaie, R Johnston, Y Gu, C Pleydell-Pearce, M Burley, J Dean & TW Clyne, *Indentation Plastometry of Welds,* Adv. Eng. Mats., **2022**, 2101645, https://doi.org/10.1002/adem.202101645.
13. M Warwick, H Vaka, CZ Fang, J Campbell, J Dean & TW Clyne, *Use of Profilometry-Based Indentation Plastometry to Study the Effects of Pipe Wall Flattening on Tensile Stress-Strain Curves of Steels,* Steel Res. Int., **2023**, 94, https://doi.org/10.1002/srin.202200920.
14. YT Tang, JE Campbell, M Burley, J Dean, RC Reed & TW Clyne, *Use of Profilometry-based Indentation Plastometry to obtain Stress-Strain Curves from Anisotropic Superalloy Components made by Additive Manufacturing,* Materialia, 15, **2021**, 101017, https://doi.org/10.2139/ssrn.3746800.
15. TJF Southern, JE Campbell, KI Kourousis, B Mooney, YT Tang & TW Clyne, *Indentation Plastometry for Study of Anisotropy and Inhomogeneity in Maraging Steel produced by Laser Powder Bed Fusion,* Steel Res. Int., 94, **2023**, https://doi.org/10.1002/srin.202200881.
16. R Reiff-Musgrove, M Gaiser-Porter, W Gu, JE Campbell, P Lewis, A Frehn, AD Tarrant, YT Tang, M Burley & TW Clyne, *Indentation Plastometry of Particulate Metal Matrix Composites, Highlighting Effects of Microstructural Scale,* Adv. Eng. Mat., **2023**, https://doi.org/10.1002/adem.202201479.

17. M Burley, JE Campbell, R Reiff-Musgrove, J Dean & TW Clyne, *The Effect of Residual Stresses on Stress–Strain Curves Obtained via Profilometry-Based Inverse Finite Element Method Indentation Plastometry,* Adv. Eng. Mats., **2021**, 2001478, https://doi.org/10.1002/adem.202001478.

18. S Ooi, R Reiff-Musgrove, M Gaiser-Porter, M Steinbacher, I Griffin, JE Campbell, M Burley, CM Warwick, H Vaka & TW Clyne, *PIP Testing for Characterization of Case Hardened Steels,* Adv. Eng. Mats., **2022**, 2201512, https://doi.org/10.1002/adem.202201512.

19. JE Campbell, M Gaiser-Porter, W Gu, S Ooi, M Burley, J Dean & TW Clyne, *Indentation Plastometry of Very Hard Metals,* Adv. Eng. Mats., **2022**, 2101398, https://doi.org/10.1002/adem.202101398.

20. R Reiff-Musgrove, W Gu, JE Campbell, J Reidy, A Bose, A Chitrapur, YT Tang, M Burley & TW Clyne, *Effect of Relatively Low Levels of Porosity on the Plasticity of Metals and Implications for Profilometry-Based Indentation Plastometry (PIP),* Adv. Eng. Mats., **2022**, https://doi.org/10.1002/adem.202200642.

21. TW Clyne, JE Campbell, M Burley & J Dean, *Profilometry-based Inverse FEM Indentation Plastometry (PIP),* Adv. Eng. Mats., **2021**, 21004037, https://doi.org/10.1002/adem.202100437.

22. H Tammpere, PJ McKeown, JR Miller, C Fang, E Curtis, M Gaiser-Porter, M Burley, JE Campbell, M Artiles, YT Tang, S Utada, RC Reed & TW Clyne, *Profilometry-based Indentation Plastometry at High Temperature (HT-PIP),* Adv. Eng. Mats., **2024**, https://doi.org/10.1002/adem.202301073.

23. PJ McKeown, JR Miller & TW Clyne, *Effects of Creep in Titanium at Room Temperature during Tensile and Profilometry-based Indentation Plastometry Testing,* Adv. Eng. Mat., **2025**, https://doi.org/10.1002/adem.202402645.

24. TW Clyne, *Analysis of Creep-Dominated Tensile Stress-Strain Data,* Int. J. Mech. Sci., 295, **2025**, https://doi.org/10.1016/j.ijmecsci.2025.11029.

25. SJ Zenobia & GL Kulcinski, *Retention and Surface Pore Formation in Helium-Iplanted Tungsten as a Fusion First Wall Material,* Fusion Science and Technology, 56, **2009**, 352-360, https://doi.org/10.13182/fst09-a8927.

26. ZH Wang, KX Zhao, WM Chen, XD Chen & LY Zhang, *Phase transformation research of fusion reactor first wall material tungsten,* Applied Thermal Engineering, 59, **2013**, 498-503, https://doi.org/10.1016/j.applthermaleng.2013.06.017.

27. JV Vas, JQ Pan, NL Wang, JH Xu, R Medwal, M Mishra, JY Pae, MV Matham, LCK Paul & RS Rawat, *Plasma processed tungsten for fusion reactor first-wall material,* J. Mat. Sci., 56, **2021**, 10494-10509, https://doi.org/10.1007/s10853-021-05917-y.

28. K Tsuchida, T Miyazawa, A Hasegawa, S Nogami & M Fukuda, *Recrystallization behavior of hot-rolled pure tungsten and its alloy plates during high-temperature annealing,* Nuclear Materials and Energy, 15, **2018**, 158-163, https://doi.org/10.1016/j.nme.2018.04.004.

29. K Wang, Y Li, X Zan, LM Luo, JQ Liu & YC Wu, *Inhomogeneous deformation substructure and its effect on the recrystallization behavior of yttria dispersion-strengthened tungsten plate,* Nuclear Materials and Energy, 35, **2023**, https://doi.org/10.1016/j.nme.2023.101405.

30. TL Shen, Y Dai & Y Lee, *Microstructure and tensile properties of tungsten at elevated temperatures,* Journal of Nuclear Materials, 468, **2016**, 348-354, https://doi.org/10.1016/j.jnucmat.2015.09.057.

31. S Nogami, A Hasegawa, M Fukuda, M Rieth, J Reiser & G Pintsuk, *Mechanical properties of tungsten: Recent research on modified tungsten materials in Japan,* Journal of Nuclear Materials, 543, **2021**, https://doi.org/10.1016/j.jnucmat.2020.152506.

32. X Cheng, ZM Xie, XF Xie, LF Zeng, R Liu, JF Yang, XB Wu, XP Wang, CS Liu & QF Fang, *Achieving a remarkable low-temperature tensile ductility in a high-strength tungsten alloy,* Tungsten, 6, **2024**, 150-161, https://doi.org/10.1007/s42864-023-00218-0.

33. A von Müller, M Ilg, H Gietl, T Höschen, R Neu, G Pintsuk, J Riesch, U Siefken & JH You, *The effects of heat treatment at temperatures of 1100 °C to 1300 °C on the tensile properties of high-strength drawn tungsten fibres,* Nuclear Materials and Energy, 16, **2018**, 163-167, https://doi.org/10.1016/j.nme.2018.06.003.

34. XL Ma, XX Zhang, F Feng, T Wang, X Liu, JB Wang, W Lv, ST Lang, CC Ge & QZ Yan, *High-temperature tensile and thermal shock characterization of low-temperature rolled tungsten,* Nuclear Materials and Energy, 34, **2023**, https://doi.org/10.1016/j.nme.2022.101353.

35. HJ Ryu & SH Hong, *Fabrication and properties of mechanically alloyed oxide-dispersed tungsten heavy alloys,* Mat. Sci. & Eng. A, 363, **2003**, 179-184, https://doi.org/10.1016/s0921-5093(03)00641-5.

36. KH Lee, SI Cha, HJ Ryu, MF Dilmore & SH Hong, *Effect of mechanical alloying process on microstructure and mechanical properties of ODS tungsten heavy alloys,* Journal of Alloys and Compounds, 434, **2007**, 433-436, https://doi.org/10.1016/j.jallcom.2006.08.284.

37. DV Kostomarov, KS Bagdasarov & EV Antonov, *Formation of complex tungsten oxides at high temperatures,* Doklady Chemistry, 442, **2012**, 37-39, https://doi.org/10.1134/s0012500812020048.

38. A Vesel, M Mozetic & M Balat-Pichelin, *Sequential oxidation and reduction of tungsten/tungsten oxide,* Thin Solid Films, 591, **2015**, 174-181, https://doi.org/10.1016/j.tsf.2015.02.019.

39. A Litnovsky, T Wegener, F Klein, C Linsmeier, M Rasinski, A Kreter, B Unterberg, JW Coenen, H Du, J Mayer, C Garcia-Rosales, A Calvo & N Ordas, *Smart tungsten alloys as a material for the first wall of a future fusion power plant,* Nuclear Fusion, 57, **2017**, https://doi.org/10.1088/1741-4326/aa6816.

40. A Alkhamees, YL Liu, HB Zhou, S Jin, Y Zhang & GH Lu, *First-principles investigation on dissolution and diffusion of oxygen in tungsten,* J. Nuclear Materials, 393, **2009**, 508-512, https://doi.org/10.1016/j.jnucmat.2009.07.012.

41. P Pigeat, N Pacia & B Weber, *Phase Transition of Tungsten Trioxide - Alpha WO3 - Orthorhombic - Alpha' WO3 Tetragonal - and Observation of its influence upon the Oxidation Kinetics by IR Spectrometry,* Surface Science, 269, **1992**, 538-544, https://doi.org/10.1016/0039-6028(92)91305-u.

42. D Nagy & SA Humphry-Baker, *An oxidation mechanism map for tungsten,* Scripta Materialia, 209, **2022**, https://doi.org/10.1016/j.scriptamat.2021.114373.

43. P Pérez & MA Monge, *Influence of 2 (wt%) titanium addition on the oxidation resistance of tungsten,* Nuclear Materials and Energy, 31, **2022**, https://doi.org/10.1016/j.nme.2022.101172.

44. T Fu, KK Cui, YY Zhang, J Wang, FQ Shen, LH Yu, JM Qie & X Zhang, *Oxidation protection of tungsten alloys for nuclear fusion applications: A comprehensive review,* Journal of Alloys and Compounds, 884, **2021**, https://doi.org/10.1016/j.jallcom.2021.161057.

45. WMR Daoush, AHA Elsayed, OAG El Kady, MA Sayed & OM Dawood, *Enhancement of Physical and Mechanical Properties of Oxide Dispersion-Strengthened Tungsten Heavy Alloys,* Mat. Sci. & Eng. A, 47A, **2016**, 2387-2395, https://doi.org/10.1007/s11661-016-3360-7.

46. J Gibson, SG Roberts & DEJ Armstrong, *High temperature indentation of helium-implanted tungsten,* Mat. Sci. & Eng. A, 625, **2015**, 380-384, https://doi.org/10.1016/j.msea.2014.12.034.

47. D Terentyev, A Bakaeva, T Pardoen, A Favache & EE Zhurkin, *Surface hardening induced by high flux plasma in tungsten revealed by nano-indentation,* Journal of Nuclear Materials, 476, **2016**, 1-4, https://doi.org/10.1016/j.jnucmat.2016.04.007.

48. A Harris, BD Beake, DEJ Armstrong & MI Davies, *Development of High Temperature Nanoindentation Methodology and its Application in the Nanoindentation of Polycrystalline Tungsten in Vacuum to 950˚C,* Experimental Mechanics, 57, **2017**, 1115-1126, https://doi.org/10.1007/s11340-016-0209-3.

49. W Zhang, XQ Gao, PX Zhang, ZW Hu, LP Li & J Cheng, *Nanoindentation Size Effect of Tungsten Single Crystal,* Rare Metal Materials and Engineering, 46, **2017**, 3626-3632, https://doi.org/10.1016/S1875-5372(18)30048-1.

50. BD Beake, AJ Harris, J Moghal & DEJ Armstrong, *Temperature dependence of strain rate sensitivity, indentation size effects and pile-up in polycrystalline tungsten from 25 to 950 °C,* Materials & Design, 156, **2018**, 278-286, https://doi.org/10.1016/j.matdes.2018.06.063.

51. XZ Xiao, D Terentyev, A Bakaev, A Zinovev, A Dubinko & EE Zhurkin, *Crystal plasticity finite element method simulation for the nano-indentation of plasma-exposed tungsten,* J. Nuclear Materials, 518, **2019**, 334-341, https://doi.org/10.1016/j.jnucmat.2019.03.018.

52. RW Armstrong, WL Elban & SM Walley, *Nano-Indentation Hardness and Strain Hardening of Silicon, Sodium Chloride and Tungsten Crystals,* Experimental Mechanics, 62, **2022**, 359-364, https://doi.org/10.1007/s11340-021-00777-8.

53. AR Khan, A Patra, D Chaira, DA Babu & V Srinivas, *Nano-indentation, Residual Stress, and Oxidation Study of Spark Plasma-Sintered Tungsten Alloys,* J. Mats. Eng. & Performance, 33, **2024**, 5223-5235, https://doi.org/10.1007/s11665-023-08358-7.

54. TJF Southern, JE Campbell, C Fang, A Nemcova, A Bannister & TW Clyne, *Use of Hardness, PIP and Tensile Testing to Obtain Stress-Strain Relationships for Metals,* Mech. of Mats., 187, **2023**, 104846, https://doi.org/10.1016/j.mechmat.2023.104846.

55. L Esposito & N Bonora, *A primary creep model for Class M materials,* Mat. Sci.& Eng. A, 528, **2011**, 5496-5501, https://doi.org/10.1016/j.msea.2011.03.069.

56. R Sandström, *Basic model for primary and secondary creep in copper,* Acta Materialia, 60, **2012**, 314-322, https://doi.org/10.1016/j.actamat.2011.09.052.

57. X Li, SR Holdsworth, E Mazza & E Hosseini, *Creep behaviour of AISI 316H stainless steel under stress-varying creep loading conditions: primary creep regeneration,* Materials at High Temperatures, 36, **2019**, 240-252, https://doi.org/10.1080/09603409.2018.1523295.

58. G Zilberstein, *Creep properties of non-sag tungsten recrystallized in stagnant oxygen-doped argon,* Int. J. Refractory Metals & Hard Materials, 16, **1998**, 71-75, https://doi.org/10.1016/s0263-4368(98)00007-9.

59. J Webb, S Gollapudi & I Charit, *An overview of creep in tungsten and its alloys,* Int. J. Refractory Metals & Hard Materials, 82, **2019**, 69-80, https://doi.org/10.1016/j.ijrmhm.2019.03.022.

60. C Wang, DB Chen, Y Zhou, ZM Xie, QF Fang, SF Wen & CZ Yan, *Microstructures, Thermal and Mechanical Properties of Pure Tungsten-A Comparison Between Selective Laser Melting and Hot Rolling,* Chinese Journal of Mechanical Engineering, 35, **2022**, https://doi.org/10.1186/s10033-022-00712-5.

61. C Bocking & IR Christie, *Gold Electroplating - A Brief Overview,* Interdisciplinary Science Reviews, 17, **1992**, 239-243, https://doi.org/10.1179/030801892791925484.

62. TR Walton, *Characterisation of Electroplated Gold Coatings for Dental Applications: Estimation of Thickness Using Non-Destructive Electron-Probe Microanalysis Related to Plating Time,* Coatings, 11, **2021**, https://doi.org/10.3390/coatings11080874.

63. R Takagi & T Liu, *Lubrication of Bearing Steels with Electroplated Gold under Heavy Loads,* Asle Transactions, 11, **1968**, 64-&, https://doi.org/10.1080/05698196808972209.

64. GA Fried, XD Wang & KW Hipps, *Gold-coated Tungsten Tips for Scanning-Tunneling Microscopy,* Review of Scientific Instruments, 64, **1993**, 1495-1501, https://doi-org/10.1063/1.1144069.

65. VN Ageev, YA Kuznetsov & ND Potekhina, *Temperature and concentration effects in electron-stimulated desorption of sodium atoms from sodium layers adsorbed on tungsten coated with a gold film,* Physics of the Solid State, 50, **2008**, 1585-1591, https://doi.org/10.1134/s1063783408080337.

66. D Duhl, KI Hirano & M Cohen, *Diffusion of Iron, Cobalt and Nickel in Gold,* Acta Metallurgica, 11, **1963**, 1-&, https://doi.org/10.1016/0001-6160(63)90119-6.

67. H Okamoto & TB Massalski, *Phase Relationships and Thermodynamic Modeling in Several Binary Systems based on Gold,* Journal of Metals, 36, **1984**, 57-57,

68. ZY Zhou, YM Ma, QF Han & YL Liu, *Solubility, permeation, and capturing of impurity oxygen in Au/Ag: A comparative investigation from first-principles,* Computational Materials Science, 114, **2016**, 79-85, https://doi.org/10.1016/j.commatsci.2015.11.023.

69. H Kipphardt, T Dudzus, KA Meier, S Recknagel, M Hedrich & R Matschat, *Measurement of oxygen and nitrogen in high purity metals used as national standards for elemental analysis in Germany by classical carrier gas hot extraction (HE) and HE after activation with photons,* Materials Transactions, 43, **2002**, 98-100, https://doi.org/10.2320/matertrans.43.98.

70. TS Yang, Y Zhang, YA Cai & H Tian, *Effect of processing parameters on anodic nanoporous tungsten oxide film structure and porosity for hydrogen detection,* Journal of Materials Research, 29, **2014**, 166-174, https://doi.org/10.1557/jmr.2013.369.

71. J Gupta, H Shaik & KN Kumar, *A review on the prominence of porosity in tungsten oxide thin films for electrochromism,* Ionics, 27, **2021**, 2307-2334, https://doi.org/10.1007/s11581-021-04035-8.

72. AY Hu, ZS Jiang, CG Kuai, S McGuigan, D Nordlund, YJ Liu & F Lin, *Uncovering phase transformation, morphological evolution, and nanoscale color heterogeneity in tungsten oxide electrochromic materials,* J. Materials Chemistry A, 8, **2020**, 20000-20010, https://doi.org/10.1039/d0ta06612e.

73. Y Abe, Y Kadowaki, M Kawamura, KH Kim & T Kiba, *Two-color electrochromic devices using a tungsten oxide and nickel oxide double layer,* Jap. J. Applied Physics, 62, **2023**, https://doi.org/10.35848/1347-4065/aca4b1.